APPROACH FOR THE AERODYNAMIC OPTIMIZATION OF THE TWIST DISTRIBUTION OF ARBITRARY WING GEOMETRIES ON CONCEPTUAL AIRCRAFT DESIGN LEVEL

T. Effing*, F. Peter†, E. Stumpf*, M. Hornung†
* RWTH Aachen University, Institute of Aerospace Systems, Wuellnerstr. 7, 52062 Aachen, Germany
† Bauhaus Luftfahrt e.V., Willy-Messerschmitt-Str. 1, 82024 Taufkirchen, Germany

Abstract

This paper presents an approach for consciously tailoring the lift distribution of a given wing geometry in early stages of aircraft design. Based on Top Level Aircraft Requirements and minimal user input, conceptual aircraft design suites such as the MICADO environment, an RWTH Aachen University (ILR) in-house development, generally enable the design of consistent aircraft. This includes the design of wing geometries based on handbook methods. For these, the twist distribution of a wing is often neither a required input nor an output. Although available in MICADO's geometric data to allow detailed analysis, the twist distribution for both clean sheet and reference aircraft designs is kept constant during the design loop. As a result, the twist is not intentionally adjusted despite its direct relationship to the lift distribution and the induced drag. For this reason, an approach is developed and incorporated in MICADO that adjusts the twist to match a given target lift distribution. First, the course of the development of the approach is discussed. This includes not only the initial idea and its implementation but also adjustments based on first results. The final approach foresees an iterative adjustment of the twist on given wing sections to match a target lift distribution; this is done using results from DLR's multi-lifting-line code LIFTING_LINE. To judge the plausibility of the resulting twist distributions, a 3D panel method is applied next. However, since no advantages can be achieved by this, LIFTING_LINE will be the default method to keep computational effort as low as possible. To show robustness and versatile usability of the approach, tool-specific studies are presented; these demonstrate, e.g., the applicability for different wing geometries and target lift distributions. Finally, the impact of incorporating the new method into MICADO and thereby matching an elliptical lift distribution is analyzed. Although significant potential in terms of trip fuel reduction is revealed for a short-range reference design, this does not hold for the clean sheet design. For the latter, various effects on both aerodynamics and structures lead to poorer overall aircraft performance. This indicates the need for more exhaustive studies to find the optimal compromise between the different disciplines in aircraft design. However, the presented approach simplifies the future setup of such studies.

Keywords: Conceptual aircraft design, MICADO, Lift distribution, Wing aerodynamics

1. INTRODUCTION

Conceptual and preliminary aircraft design environments often use simple methods that are aimed at reproducing realistic aircraft characteristics as accurately as possible. For the wing, these characteristics mainly include the estimation of aerodynamic performance and mass. The lift distribution of a wing affects both of these aspects and therefore has a major role in the common trade-off between aerodynamic potential and structural requirements. Often, from an aerodynamic point of view, an elliptical lift distribution is targeted, which is considered beneficial for induced drag since the early 20th century [1]. However, the structure of the wing must be sized accordingly to bear the occurring loads. This opens up a large design space that must be explored to identify an overall optimum with respect to the aircraft's fuel consumption. The paper at hand presents a straight forward approach to modify the twist of a known wing in order to approximate a target lift distribution using a multi-lifting-line code. This target distribution can either be defined by the user or known from higher order calculation methods. The other parameters defining the geometry of the wing (i.e. planform, dihedral and airfoils) have to be known in advance and remain unchanged. While the approach does not aim at an optimization, but the approximation to an input lift distribution, an external change of that input allows the application in an optimization process.

2. FUNDAMENTALS

Conceptual aircraft design can employ different tools to assess the aerodynamic characteristics of a wing. While for early stages and conventional geometries, semi-empirical methods (e.g. Torenbeek [2] or Raymer [3]) are suitable, studies, which require sensitivities for the specific geometry of the wing or deal with unconventional configurations, have to apply other methods. The application of analytical methods has proven to be useful for obtaining

doi: 10.25967/550197

aerodynamic performance data for the wing, while being computationally cheap enough to analyze large design spaces. Commonly, these tools are integrated in a conceptual aircraft design environment such as MICADO[1], providing a new set of aerodynamic performance data for each iteration of the loop. The principle setup of MICADO, the aircraft design software, the approach presented in this paper is planned to be incorporated in, is shown in Fig. 1.

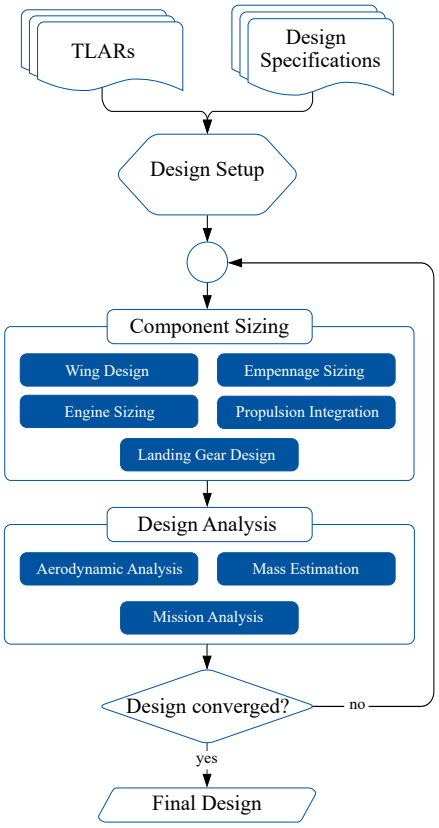

FIG 1. MICADO process chain

After the user defines basic information for the design task, several tools are executed in order to size the aircraft components. Subsequently, the design analysis tools are executed, of which the aerodynamic analysis is one. The design loop is iterated until convergence for a small number of major design parameters is achieved. Although many aerodynamic effects can sufficiently be estimated with semi-empirical methods (e.g. for viscous drag taking into account wetted area and form factors), the lift distribution is dependent on the specific geometry of the wing. When analyzing a wing geometry that involves not only high level parameters, such as aspect ratio and span, but also multiple wing segments or non-planar features, it is critical to tailor the lift distribution well to obtain meaningful aerodynamic performance results. A brief discussion of the role of the lift distribution, and suitable methods for its calculation, is done in the following sections.

[1] Multidisciplinary Integrated Conceptual Aircraft Design and Optimization environment [4, 5]

2.1. Relevant influences on lift distribution

The goal of an aerodynamic analysis is to provide both drag data for a subsequent mission analysis and loads for a structural design. To enable the mission analysis for any flight condition that might occur during the mission, aerodynamic data for the entire flight envelope have to be calculated. Therefore a set of parameters determining the flight condition have to be defined. For this study, these parameters are:

- Mach number (Ma),
- angle of attack (AoA),
- flight altitude (defined by Reynolds number).

Various possibilities exist to define the wing's geometry. The selected approach is common to many simple aerodynamic analysis tools and is specifically the one used in MICADO. Here, the geometry of the wing in flight shape is defined by sections, with specific airfoils, chord and twist. Two sections create a segment and their position to each other is defined by the segment span, leading edge angle and dihedral. The wing can then be built up using several segments. The empennage surfaces are defined in the same manner and positioned in relation to the wing. As described earlier, for the presented approach, only the twist of the wing is varied to change the lift distribution. All other parameters are unaffected.

2.2. Influence of lift distribution in aircraft design process

The principle goal of an aerodynamic analysis is to calculate the forces exerted by the airflow on the aircraft. The resulting drag is of primary interest for the aircraft performance calculation. In MICADO, drag is composed of viscous ($C_{\mathrm{D,visc}}$), induced ($C_{\mathrm{D,ind}}$), and wave ($C_{\mathrm{D,wave}}$) drag:

$$C_{D,total} = C_{D,visc} + C_{D,ind} + C_{D,wave} \tag{1}$$

While the focus of this paper is on the induced drag, which is strongly influenced by the lift distribution, it should be mentioned that the wave drag is calculated with a method combining Lock's fourth power law [6] with Korn's relation [7]. Therefore, the local lift coefficient (C_{l}) of a spanwise section of the wing is taken into account for the wave drag calculation, which is consequently also influenced by the lift distribution. The viscous drag, which also includes miscellaneous drag such as parasite drag, is determined using a method presented by Raymer [3]; this method only takes into account the global lift coefficient (C_{L}) of the entire airframe. Thus, in the process applied in this work, changing local lift distributions are not expected to affect the viscous drag component.

Besides the influence on the drag, the lift distribution determines the location where the lift force is exerted on the wing, thereby defining the load distribution. A major result of this is the impact on the

root bending moment of the wing, which increases the further outwards the center of pressure (CoP) is acting on the wing. Hence, the overall aircraft optimum of the adjustment of the lift distribution will not only be defined by the minimum of drag but also by consideration of the weight of the wing structure resulting from the aerodynamic loads location. The aero-structural interaction is one of the main drivers necessitating an iterative execution of the tools as shown in Fig. 1. This incorporates snowball effects, which is necessary for consistent aircraft design.

2.3. Relevant Methods

As stated before, there is a need in conceptual aircraft design for methods that are sensitive to specific geometric changes of the wing, while being fast and stable enough to enable large design space explorations. Potential flow analysis methods satisfy this need, but trade aerodynamic accuracy for computational speed by neglecting viscosity and compressibility. Different applications of the potential flow concept are available, of which the multi-lifting-line and the three dimensional (3D) panel methods are discussed in this paper.

2.3.1. Multi-lifting-line approach

The basic idea of this potential-theoretical approach is to divide the lifting surface(s) into span- and chordwise panels and to apply both the concept of circulation and the Kutta-Joukowski theorem. Placing and subsequently solving a vortex system on each of these panels enables the calculation of (total and spanwise) lift, pitching moment, and induced drag. In this approach, the wing's airfoils are only considered by their camber line. The actual thickness of the airfoil is neglected. The method is an advancement relative to the vortex-lattice method (VLM), e.g. implemented in AVL[2] [8], because the spanwise distribution of circulation of each vortex is not constant but is described by a quadratic function. [9] A prominent example of this approach is the LIFTING_LINE (LILI) code [10], which is used for this work. It is applicable to subsonic compressible flow conditions by using Göthert's 3D extension [11] of the Prandtl-Glauert rule [12].[3]

2.3.2. 3D panel method

In contrast to VLM or the multi-lifting-line method, 3D panel methods consider the three dimensional shape of the modelled components. For the airfoil, this means that the thickness along the span is taken into account, usually by applying doublets as potential flow elements, e.g., to model the flow of the upper and lower side of an airfoil. Different 3D panel methods are available, of which PanAir [14] is one of earliest and best known implementations. Other examples are the (license-)free PANUKL [15] and VSPAero [16] codes as well as PMARC [17] (free, but licensed program by NASA). The latter is an example for a solver where in addition to the potential flow analysis, boundary layer models have been added to include viscous effects. PMARC is furthermore relevant, since it was used in a study relevant for this paper (see Sect. 3).

[2] Athena Vortex Lattice

[3] At given total lift and compared with higher order methods such as Reynolds-averaged Navier-Stokes (RANS) computations, LILI also provides reasonable results for transonic flow conditions [13].

3. DERIVED APPROACH

Currently, the adaptation of the twist distribution is not a part of MICADO. This leaves the following options for the reference design and the clean sheet design:

- Reference design: Either use a given or a common twist distribution; these can, e.g., be found in Obert [18].
- Clean sheet design: Neglect the option to influence the local lift via twist (i.e. zero twist).

However, both ways lead to the fact that possible potentials of a tailored lift distribution either remain unused or can only be explored via time-consuming manual adaptation and subsequent studies.

A promising approach of achieving arbitrary lift distributions by applying twist was presented by Lane et al. [19]. This approach foresees a superimposition of lift deltas due to different twist distributions and subsequently the calculation of the required twist function weights. Ultimately, this yields an optimal twist to approximate a target lift distribution. Although a different approach has been derived in the paper at hand, it is important to highlight that the authors from Ref. [19] used two different solving methods within their approach, namely AVL and PMARC (see Sect. 2.3). For both methods, the desired lift distributions could be achieved; nonetheless, the different solving methods lead to very different twist distributions to produce an approximated elliptical lift distribution. Whereas the twist resulting from AVL shows a wavelike behavior with a steep negative gradient in the outer wing area, the results obtained with the 3D panel method PMARC show a nearly constant but reasonable negative twist gradient. This fact will be revisited in Sect. 3.2.2.

3.1. Initial idea and implementation

The goal of the presented approach is to modify the twist of known wing sections in order to achieve a predefined lift distribution. Figure 2 shows the general sequence of the approach.

For the initial/current wing geometry and the design flow conditions (i.e. global AoA and Mach number), LILI is executed and the lift distribution, consisting of local lift coefficient values multiplied with the local chord ($C_l \cdot l$), is calculated. The result is compared

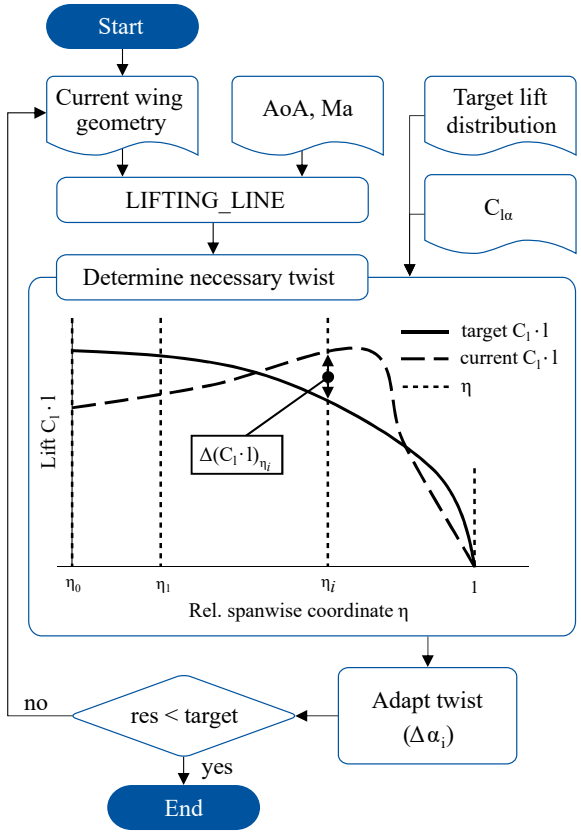

FIG 2. Basic process of twist adaptation

with the target lift distribution. This distribution can be an input from literature (e.g., elliptical or bell-shaped), which is then scaled to a target global lift coefficient, or an output from a higher-order calculation method such as RANS results. For efficient adaptation of the target lift distribution, a special case of a Fourier sine series definition of the lift distribution[4] is used [21]:

$$L(\Theta) = 2b\rho v_\infty^2 \frac{C_L}{\pi\Lambda}(\sin(\Theta) + B_3 \sin(3\Theta)). \quad (2)$$

Hence, the local wing section lift $L(\Theta)$ is defined by the wingspan b, the air density ρ, the flight speed v_∞, the global lift coefficient C_L, the aspect ratio Λ, the Fourier coefficient B_3, and $\Theta = \text{acos}(-2y/b)$. Using Eq. (2), the target lift distribution can be varied through the Fourier coefficient B_3; for example, $B_3 = 0$ leads to the known ellipse, whereas $B_3 = -1/3$ results in a bell-shaped distribution.

Next, for each relative section position η_i, the delta of local lift $\Delta(C_l \cdot l)_{\eta_i}$ is determined. Using either a specific or a default local lift gradient (e.g. $C_{l\alpha} = 2\pi$), the necessary change in AoA is calculated and the twist is adapted according to the following equation:

$$\Delta\alpha = \frac{\Delta(C_l \cdot l)}{C_{l\alpha} \cdot l}. \quad (3)$$

[4]This special case with Fourier coefficients $B_n = 0$ for all $n \neq 3$ is recommended for use when designing wings for minimum induced drag [20].

The amount of local lift deviation is then compared with a predefined residuum. If the deviation is small enough, the process is terminated, if not, the adapted wing geometry is analyzed again with LILI, and the process is repeated.

3.2. Improvements based on first results

To explore the functionality of the initial approach, the CeRAS short-range aircraft (CSR-01) is used.[5] Figure 3 shows the kinked planform, which features a span of $b = 34$ m and a reference area of $S_{ref} = 122.4\,m^2$.

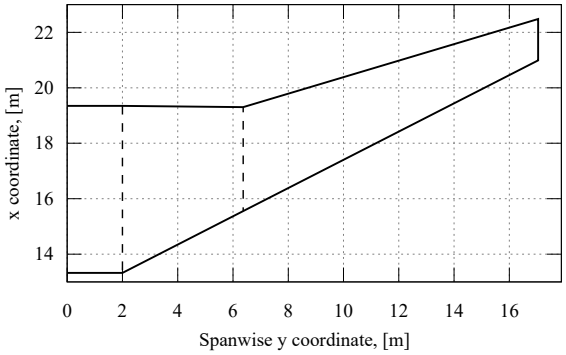

FIG 3. Planform of the CSR-01 reference wing

As illustrated in Fig. 3, the reference wing consists of three segments; this leads to four given control points for the adjustment of the twist distribution. Since the aerodynamic performance during cruise conditions is of major interest, the following studies are performed at $Ma_{cr} = 0.78$ and target an elliptical lift distribution. Using the initial approach, this leads to the converged results depicted in Fig. 4.

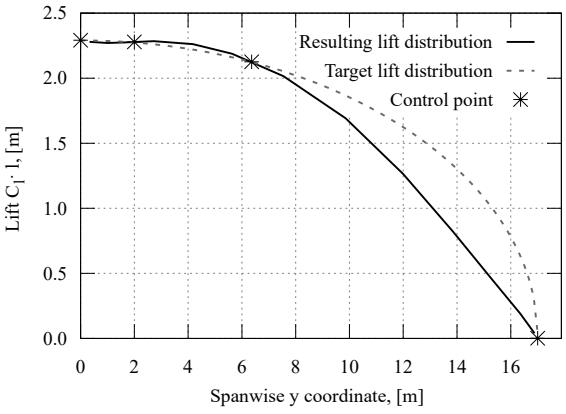

FIG 4. Results for initial approach

It can be seen that the curves match at the given control points; this leads to convergence using the residual mode described in Sect. 3.1. Between the control points, however, the lift distributions deviate. This especially applies to the outer wing segment,

[5]The "Central Reference Aircaft data System" database provides reference aircraft data for public access and enables communication within the research community [22, 23].

where the distance between the control points is particularly large. Two questions arise from these observations:

1) Is the chosen method for calculating the residual suitable for this use case?
2) Even if a different residual mode is available, is the given number of segments and thus the number of control points sufficient to achieve a better approximation of the target lift distribution?

To address these questions, adjustments are implemented in the approach, which are described in the following section.

3.2.1. Adjustments to initial approach

Instead of relying only on the residuals at the respective control points, the so-called root-mean-square error is utilized to calculate the residual ϵ_i for every segment i:

$$\epsilon_i = \sqrt{\frac{1}{N_i} \cdot \sum_{n=1}^{N_i} \Delta(C_l \cdot l)^2} \tag{4}$$

with N being the number of spanwise panels defined by the solving method used. On the basis of pre-studies, the default value of the residual is set to ϵ = 0.02. This new approach prevents convergence if the deviations between two control points are as large as, e.g., in Fig. 4. Therefore, this first adjustment prevents the process to converge, since the number of control points is not sufficient to minimize the deviations in the outer wing segment. To minimize the required user interaction, an (optional) automatized adaptation of the number of wing segments is implemented. If the differences in the lift distributions do not fall below a specified residual after a certain number of iterations, the first outer segment that lies above the residual is split. This is done by interpolating the relevant geometric parameters, such as the adjacent airfoils. The linear interpolation does not change the geometry of the wing and thus only creates a new control point for adjusting the twist.

3.2.2. Results with adjusted approach

For the same input that led to the initial results in Fig. 4, the results after the described adjustments are shown in the upper part of Fig. 5.

It is obvious that the resulting lift distribution matches the target lift distribution. On a standard desktop computer, convergence is obtained after 15 iterations and in less than one minute; this is achieved by automatically adding a control point every second iteration. Therefore, the method is suitable for integration into a conceptual aircraft design environment like MICADO. The resulting twist distribution is illustrated

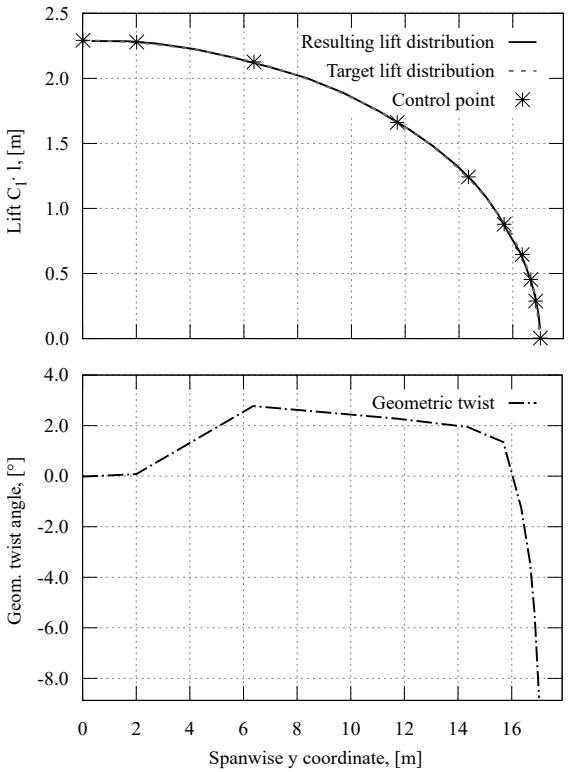

FIG 5. Results with LILI after adjustments

in the lower part of Fig. 5.[6] It can be observed that after an initial increase to the kink at about y = 6.4 m, the twist angle decreases slightly before a very high negative gradient occurs. This is attributed to the hard criterion of matching the ellipse even in the outer region and thus at values approaching 0. This fits the necessity for the high number of control points in the outer wing area (see upper part of Fig. 5). In particular this gradient, and thus the course in the wing tip region, does not meet expectations compared to more realistic twist distributions such as those found in Obert [18]. For example, the twist distribution in flight shape for an Airbus A320, which is similar to the CSR-01, is given with the values listed in Table 1.

TAB 1. Airbus A320 twist values from Ref. [18]

Position	η	Twist, [°]
Root	0.12	$\approx$ 3.5
Kink	0.37	$\approx$ 0.5
Tip	1.00	$\approx$ -0.5

Interestingly, the results in the lower part of Fig. 5 show qualitatively similar behavior to the results obtained by Lane et al. [19] using AVL and thus a similar solution procedure. In contrast and as already highlighted in the beginning of Sect. 3, the authors in Ref. [19] achieved more reasonable results by using the same approach but with PMARC instead of AVL; therefore, the correlation between wing geometry

[6] Every figure in this work showing any kind of local twist angle distribution already contains the incidence angle of the wing.

and lift is apparently better represented with a panel method. Without going into further detail, the authors hypothesize that one possible reason is the lack of consideration of the airfoil thickness in the vortex lattice method [19].

Consequently, to investigate this hypothesis, the next step is to further extend the approach from this work by a 3D panel method.

3.3. Implementation of 3D panel method

To provide the best possible comparison with the results from Ref. [19], PMARC would naturally be the first choice; unfortunately, during development of this approach, the program was not available due to licensing. Therefore, PANUKL is implemented; this free tool comes with automatized grid generation, is—similar to LILI—script-based and thus easy to implement in the approach. Most importantly, it comes with consideration of the airfoil thicknesses and enables to investigate whether or not this is the crucial factor for the final form of the twist distribution. The results achieved with PANUKL are illustrated in Fig. 6.

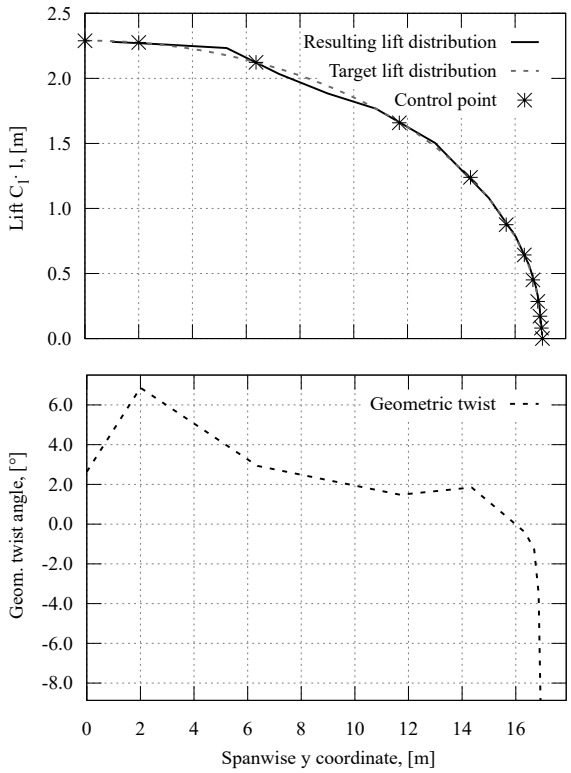

FIG 6. Results achieved with 3D panel method

In the upper part of Fig. 6 it can be seen that the converged lift distribution slightly deviates from the target distribution. Nevertheless, it is first noted that the approach also works with the chosen 3D panel method. However, the residuals slightly oscillate and require some iterations to stabilize after adding a new control point and subsequently distributing new panels. Therefore, the number of iterations after which a control point is added has to be adapted from two to five. This not only leads to an increased iteration count of 47 and an almost fivefold increase in computational costs but also to more control points before convergence is reached. In addition, the resulting twist distribution in the lower part of Fig. 6 reveals a similar course to LILI in the outer wing area; consequently, the sole consideration of the airfoil thickness does not seem to be the decisive point when it comes to more realistic twist distributions. Therefore, the next step would be to investigate the effect of viscosity, which—in contrast to PANUKL—PMARC takes into account; this will be done once PMARC is available. For the further course of this work, however, LILI will be used, since no advantages can be achieved with PANUKL.

On the basis of former observations, the resulting twist distributions are considered as tool-specific twist distributions, which lead to a physical feasible lift distribution. Thus, the course of the resulting twist distributions is no longer discussed in the next sections. Nonetheless, the authors emphasize that these should not be used as input for higher order methods such as RANS. What further research the authors intend to conduct in this regard in the future will be revisited in the summary in Sect. 6.

4. TOOL-SPECIFIC STUDIES

This chapter presents various tool-specific studies to highlight both robustness and versatile usability of the new module. First, the influence of the user-defined angle of attack is discussed (Sect. 4.1). Then, the behavior of the method for different initial twist distributions is briefly analyzed (Sect. 4.2). Subsequently, different target lift distributions (Sect. 4.3) as well as an aircraft with both different TLARs and a different wing geometry (Sect. 4.4) are investigated.

4.1. Variation of angle of attack

Since the AoA is unknown in this early stage of aircraft design, the user has to choose one in an expected range. To ensure that this initial guess does not significantly affect the resulting lift distribution, the test case from Sect. 3.2 is repeated for $-1^\circ \leq AoA \leq 3^\circ$ with $\Delta AoA = 1^\circ$. The results are shown in Fig. 7.

The upper part of Fig. 7 indicates that the choice of the angle of attack has no influence on the approximation of the lift distribution. Rather, the variation in angle of attack is compensated with the adaptation of the incidence angle of the wing. This can be seen in the almost parallel shift of about 1° of the single twist distributions in the lower part of Fig. 7. Nonetheless, it is not a constant offset of exactly 1° and thus not a perfect compromise between AoA and twist. As communicated by the German Aerospace Center (DLR), this is due to improvements in the update to LILI V3.0, more precisely in the definition of the

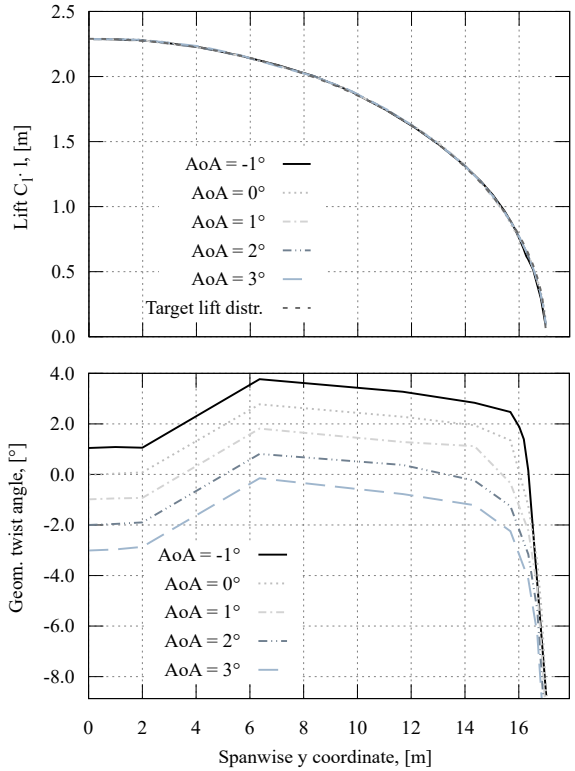

FIG 7. Results for different predefined AoAs

coordinate systems, the removal of approximations for small angles, and handling of the control points for the kinematic flow condition (for the bound vortices). Deviations in the outer wing area result from slightly different iteration numbers and the associated number of control points due to the automatic segmentation approach (see Sect. 3.2.1).

The results show that the predefined AoA does not affect the output of the method significantly; thus, the user can either choose an angle of attack in an expected range or even feed back results from the design loop, e.g., the mean angle of attack during the mission.

4.2. Variation of initial twist

For an automatized approach, robustness is key for integration into an iterative process chain such as MICADO. Hence, changes in the initial twist distribution due to a previous iteration, i.e., the twist distribution with which the method starts, must not change the output of the current iteration. To simulate this, four test cases with different initial twist distributions are analyzed; these twist distributions as well as the resulting lift and twist distributions are shown in Fig. 8.

Starting with the upper part of Fig. 8, it becomes clear that a wide variety of initial twist distributions are used. Of course, this is only to check the robustness of the method and not to specify realistic twist distributions. Nonetheless, the given twist distributions have no influence on the resulting lift and twist distributions as can be seen in the middle and lower part of Fig. 8. Therefore, the method is robust to changes in the initial twist distribution, making it suitable for use in an iterative aircraft design environment such as MICADO.

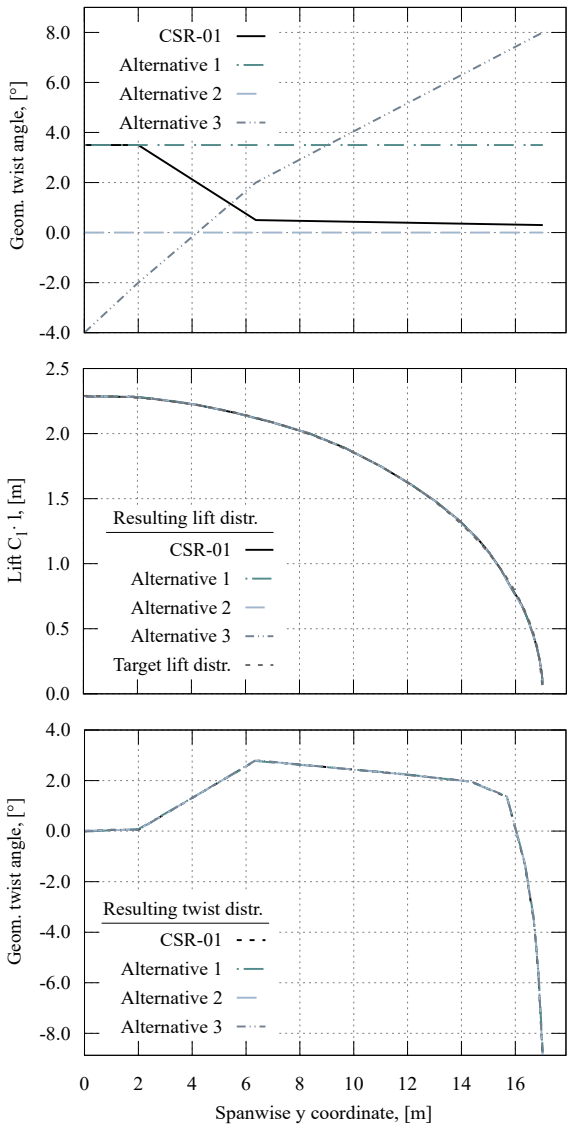

FIG 8. Results for different starting twist distributions

4.3. Application of different target lift distributions

Until now, the target lift distribution has always been the ellipse. In conceptual aircraft design, however, the effect of different lift distributions should be investigated to find a global optimum, e.g. taking into account aerodynamics and structures. To analyze the capability of the method to approximate other lift distributions, two more target distributions are defined using Eq. (2): A bell-shaped one and one with a random B_3 coefficient between the ellipse and the bell-shaped lift distribution. The different targets as well as the resulting lift distributions are shown in the upper diagram of Fig. 9.

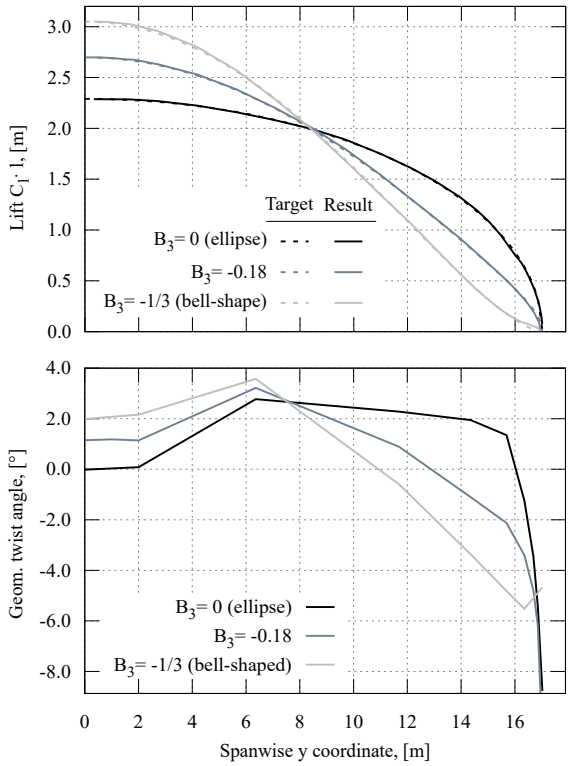

FIG 9. Results for different starting twist distributions

As can be seen in the upper part of Fig. 9, the method enables approximation of different target distributions; this also includes more complex ones as the bell-shaped with an inflexion. The required twist distribution for each target is depicted in the lower part of Fig. 9. It shows that the resulting twist distributions generally follow the course of the lift distribution; more precisely, if the local lift of one case is higher than that of another case, this also applies for the corresponding twist. The slight offset of the crossing point in the middle region is attributed to the chosen setting that a segment is divided in the outermost area where the residual value is still too high, and thus to the available control points.

In the future, the demonstrated functionality for approximating different lift distributions will allow studies, e.g., on the bell-shaped lift distribution in the overall aircraft design (OAD) context. This distribution is of particular interest as it actually outperforms the elliptical lift distribution in terms of minimum induced drag if the wing structure is taken into account and the wingspan is not a fixed constraint [1].

4.4. Application for different wing geometry

The presented method must not only work for one specific aircraft with its TLARs and wing geometry but for arbitrary wing geometries in CS-25 conceptual aircraft design. Thus, results for a different aircraft, namely the AVACON Research Baseline 2028 (ARB2028)[7], are presented. The planform of this aircraft is illustrated in the upper part of Fig. 10.

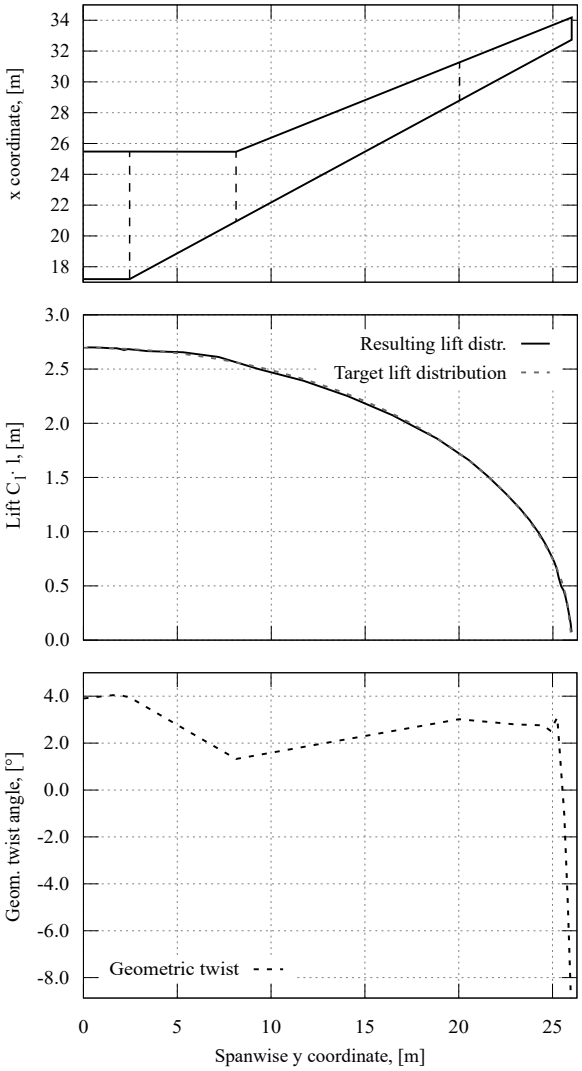

FIG 10. Results for ARB2028 wing geometry

The ARB2028 has four wing segments on each side, a wingspan of b = 52 m, and a reference area of S_{ref} = 220 m^2. In addition, it is designed for a cruise Mach number of Ma_{cr} = 0.83. In the middle diagram of Fig. 10 it is shown that the method approximates the lift distribution to the elliptical target distribution; hence, the method also works for this wing geometries. Nonetheless, the twist distribution in the lower part of Fig. 10 deviates from the one of the CSR-01 in the lower part of Fig. 5. This is to be expected, since on the relevant LILI input not only the cruise Mach number and the planform change but also the airfoils used and thus the camber line. In the wingtip area, however, the twist distribution shows similar behavior as for the CSR-01. This indicates that the criterion to perfectly match the target lift distribution even on the outer ellipse might lead to the observed behavior. In the future, further adjustments will be investigated

[7]The ARB2028 originates from the German LuFo project AVACON and is a medium-range reference aircraft with an expected technology status of the year 2028 [24].

regarding a relaxation of this criterion, especially for the outer wing region where the target lift distributions approach local lift coefficients of $C_l = 0$.

After these reflections on tool-level, the next chapter elaborates on the influence of approximated lift distributions on OAD level.

5. OVERALL AIRCRAFT DESIGN STUDIES

The overall objective of this chapter is to show the influence of approximated lift distributions on OAD level for both reference aircraft and clean sheet designs. For all studies, the Fourier coefficient is $B_3 = 0$, so that an elliptical lift distribution is targeted. In the MICADO design loop presented in Fig. 1, the method is integrated as a new module, *liftDistributionModifier* (LDM), and is executed right after the wing design. To avoid unnecessary segment splits, the automatic segment adjustment is turned off after the first iteration; this approach assumes that enough control points are available for the rest of the design loop. The assessment of the impact on aerodynamics is possible with the normal MICADO toolchain, which already includes LILI for the prediction of lift and induced drag and the semi-empirical equations described in Sect. 2.2 for the remaining drag components. To also account for detrimental effects of approximating a specific lift distribution, an ILR internal tool to calculate the structural mass of the wing on the basis of static aero-elasticity is used. This tool checks several load cases for the current lift distribution and calculates the required wing mass on the basis of stiffness matrices [25]. For each design, the analyses are structured as follows:

1) Analysis of the aerodynamics on both wing and global drag polar level;
2) Analysis of overall performance for the design mission taking into account aerodynamics, masses, and snowball effects.

First, the reference design, i.e. the design with known CSR-01 geometry, is analyzed.

5.1. Reference design

The CSR-01 is a short range aircraft with TLARs similar to an Airbus A320. The relevant key parameters are listed in Tab. 2; the planform of the wing was already introduced in Fig. 3.

TAB 2. Relevant key parameters of CSR-01 aircraft

Parameter	Unit	Value
Design range	NM	2,500
Initial cruise altitude	ft	33,000
Ma_{cr}	-	0.78
PAX	-	150

This reference aircraft is designed twice, with and without the LDM. The version without the LDM is designed with the default twist distribution shown in the upper part of Fig. 8. The lift distribution of the other version is approximated to an ellipse for a global lift coefficient of the wing of $C_{L,wing} = 0.5$ at an angle of attack of $AoA = 0°$.

5.1.1. Aerodynamics - Reference design

Starting with the aerodynamics of the wing, the polars of the induced and wave drag components are depicted in Fig. 11; the viscous drag polar is intentionally left out, since this component is only calculated for global C_L values (see Sect. 2.2).

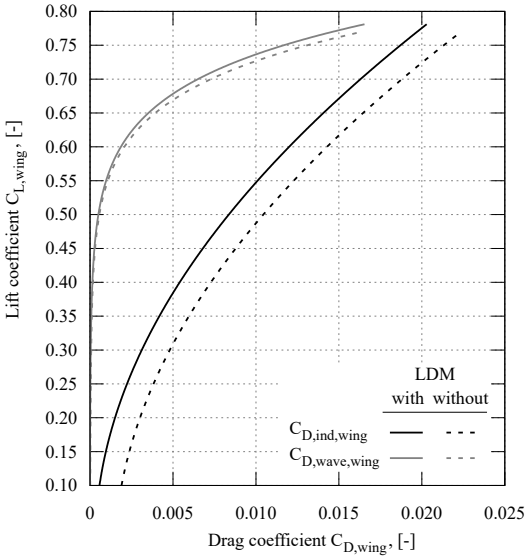

FIG 11. Wing drag polars - Reference designs

As can be seen, the usage of the LDM leads to a significantly reduced $C_{D,ind,wing}$; this can be attributed to the improved lift distribution, which is exemplified for $C_{L,wing} = 0.5$ in Fig. 12.

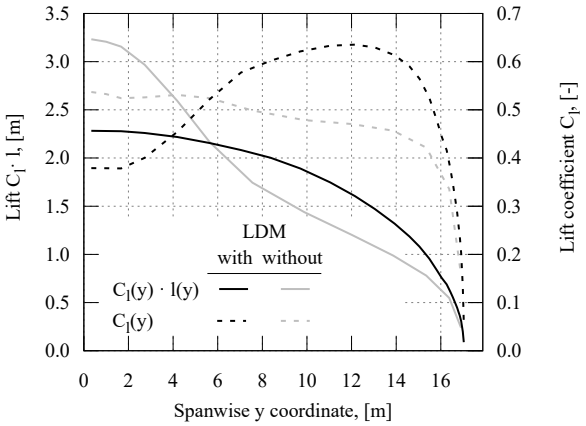

FIG 12. Lift (coefficient) distr. at $C_{L,wing} = 0.5$ - Reference designs

In contrast to the solid black curve representing the lift distribution of the LDM design, the solid grey curve is not elliptical and thus, for a fixed span,

not in the aerodynamic optimum. For $C_{L,wing}$ = 0.5, this deviation leads to a drag count reduction of $\Delta C_{D,ind,wing} \approx 21$ dc or nearly 20 %. The wave drag in Fig. 11 is slightly decreased for the LDM design due to differences in the local lift coefficient distribution; for $C_{L,wing}$ = 0.5, these differences are also shown in Fig. 12. The differences in the wave drag polar are not as significant as for the induced drag because a change of sign occurs in the delta of the lift coefficient curves; according to Korn's relation [7], the design without LDM produces more wave drag at the inboard wing, whereas the LDM design produces more wave drag at the outboard wing.

In order to classify how the effects can be transferred from wing to aircraft level, the global drag polars of all drag components are shown in Fig. 13.

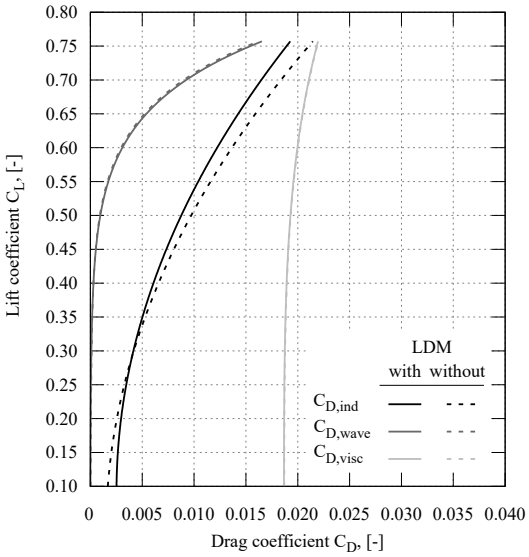

FIG 13. Global drag polars - Reference designs

As expected, the viscous drag polars show no differences (see Sect. 2.2). The benefit in the induced drag polar of the LDM wing, however, is not fully transferred to the global polar. Although there is a similar benefit for high C_L values, this benefit decreases with decreasing lift coefficients. At C_L = 0.275, the polars even cross, making the design without the approximated lift distribution more favorable in terms of induced drag. This behavior is mainly due to the automatic trim during the design loop and the resulting incidence angle of the horizontal tailplane (HTP).[8] To trim the LDM design, the incidence angle of the HTP is set to i_{htp} = -0.72°, whereas the one of the other design is set to i_{htp} = 1.44°. This results in two effects, which together explain the course of the induced drag polars in Fig. 13:

First, different values for $C_{L,wing}$ and $C_{L,htp}$ are necessary to achieve the same global C_L. This is visualized in Fig. 14.

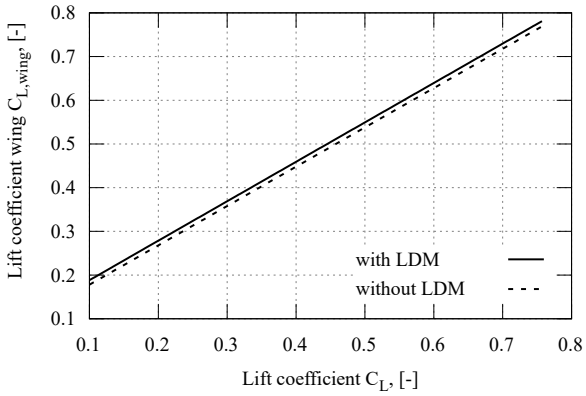

FIG 14. $C_{L,wing}$ over C_L - Reference designs

Since the LDM design consistently requires higher $C_{L,wing}$ values to achieve the same global lift coefficient, the benefit transferred from the wing polar is lower as $C_{D,ind}$ increases with increasing C_L. Nevertheless, the offset in Fig. 14 is not so significant as to explain the course of the induced drag for lower C_L values in Fig. 13. This leads to the second point. Due to differences in both the incident angle of the tailplane and the downwash of the main wing, the induced drag components of the HTP also change between the two aircraft. For a global lift coefficient of C_L = 0.1, this leads to induced drag components of the HTP of $C_{D,ind,htp} \approx 1.2$ dc (with LDM) and $C_{D,ind,htp} \approx$ -1.1 dc (without LDM), respectively.[9] Therefore, the total induced drag of the LDM design is increased by the HTP. In the design without the LDM, there is no reduction but an increase. The combination of these two effects results in the—at first glance—unexpected behavior of the induced drag polars in Fig. 13.

In addition, the wave drag is slightly increased for the LDM design. Although the respective wave drag polar at wing level is more favorable for the LDM design (see Fig. 11), this also changes due to the pitch trimming and associated wing lift coefficients required for a constant global lift coefficient (see Fig. 14).

Nonetheless, for lift coefficients relevant for cruise flight ($C_L \approx 0.5$), the LDM design benefits from the elliptical lift distribution. For the exemplary point of C_L = 0.5, the differences in Figures 12 and 13 lead to an increase of the L/D of 3.2 %. How this aerodynamic benefit influences the performance of the aircraft is analyzed next.

5.1.2. Overall performance - Reference design

One key parameter to compare aircraft designs is the trip fuel required for the design mission (TF_{dm}). To al-

[8] An automatic pitch trimming of the aircraft in cruise conditions is performed during the design iteration process. The HTP incident angle is hereby changed until the sum of moments around the y-axis for wing and HTP calculated by LILI is zero.

[9] At the HTP, negative drag components (and thus thrust) can occur when the upwash of its free vortices is (over-)compensated by the downwash of the wing [26].

low a fair comparison in MICADO, the cruise altitude profile is determined automatically within the mission analysis module with respect to an optimized specific air range; thus, not only the aerodynamics but also the engine efficiency and the aircraft mass are considered. In Fig. 15, the trajectory as well as the C_L profile of the design mission are shown.

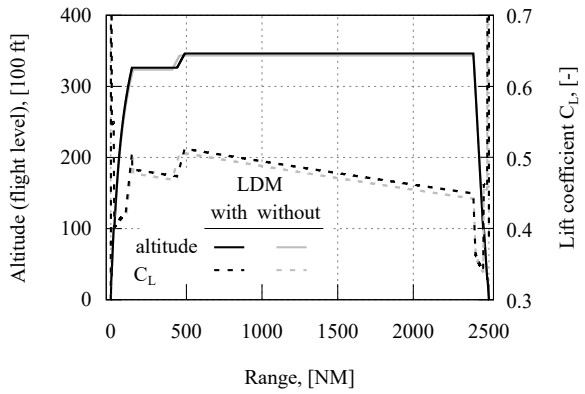

FIG 15. Altitude and lift coefficient profiles for design mission - Reference designs

The resulting altitude cruise profiles only show minor deviations between the two designs. This also holds for the typical sawtooth C_L profile; the slight shift indicates the minor change in the optimum lift coefficients, which are $C_{L,opt}$ = 0.532 for the design without LDM and $C_{L,opt}$ = 0.538 for the LDM design, respectively. For this design mission, the relative percentage changes of the LDM design compared to the design without LDM are illustrated in Fig. 16.

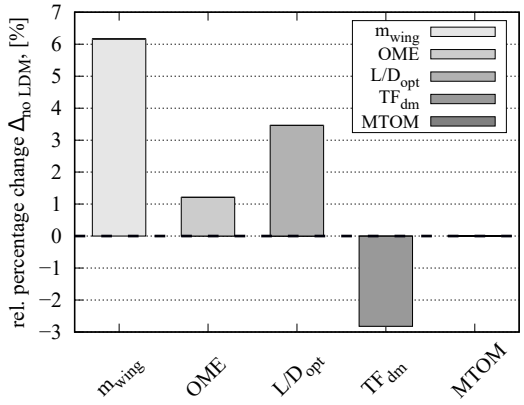

FIG 16. Relative percentage changes compared to reference design without LDM

It becomes clear that the approximation to an elliptical lift distribution comes with a significant increase in structural mass of the wing. This is due to the shift of the center of pressure as can be seen in Fig. 12. Since the CoP of the LDM design is further outboards, heavier wing structure is required to compensate the increased root bending moment (see Sect. 2.2). Including the snowball effect from the design iterations, this results in an increase of the operating mass empty (OME) of about 1.2 %. The aerodynamic benefit, however, not only increases the optimum lift coefficient but also surpasses the detrimental effect on the structure mass. As a result, the trip fuel is reduced by 2.8 %, which actually results in no increase in the maximum takeoff mass (MTOM) despite the increase in OME.

Therefore, the integration of the LDM into the design loop reveals promising potential by deliberately modifying the twist to achieve a given target lift distribution. Whether this also holds for a clean sheet design will be discussed in the next section.

5.2. Clean sheet design

For consistency, the clean sheet aircraft are also designed with the parameters listed in Tab. 2. In contrast to the reference designs, for the clean sheet designs, the modules in the component sizing block in Fig. 1 actively size the geometry. It is important to recall what was highlighted in the beginning of Sect. 3: In MICADO, no specific local twist angles are considered for a clean sheet design; hence, for the twist distribution of the design without LDM, *Alternative 2* from the upper part of Fig. 8 is used throughout the whole design loop. Since the component sizing is done with the same input parameters, no significant changes in geometry occur. The total wingspan, for example, differs by only 0.2 %. Therefore, no exhaustive comparison of the individual component parameters is conducted in this section. Of course, relevant changes are highlighted and discussed.

5.2.1. Aerodynamics - Clean sheet design

Starting again with the aerodynamics of the wing, in Fig. 17, the wing polars for the induced and wave drag components are shown.

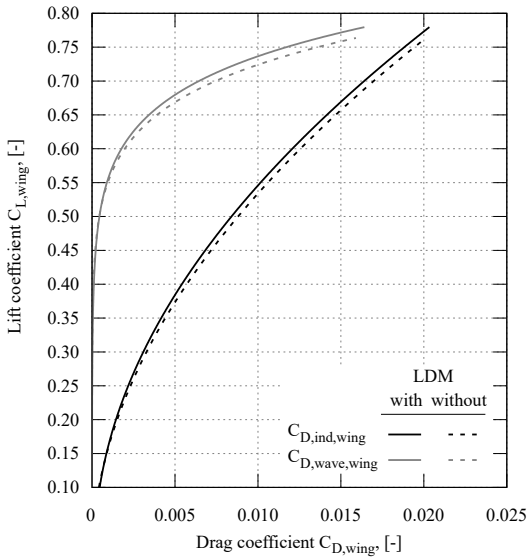

FIG 17. Wing drag polars - Clean sheet designs

While the wave drag shows similar behavior to the respective polars of the reference designs in Fig. 11, the benefit in induced drag is comparatively small. For

lower $C_{\mathrm{L,wing}}$ values, the two curves even approach each other. This is due to the local lift distributions, which are exemplary shown for two different $C_{\mathrm{L,wing}}$ values in Fig. 18.

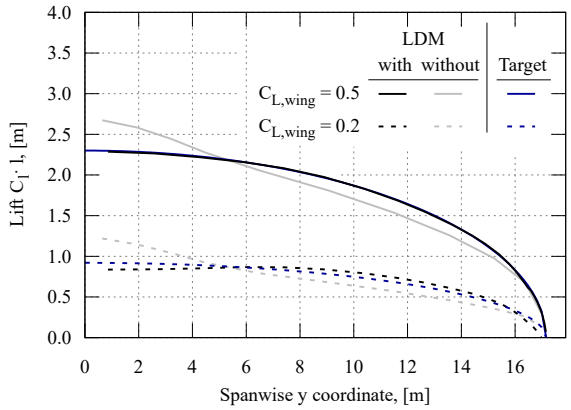

FIG 18. Lift distr. at $C_{\mathrm{L,wing}}$ = 0.2 & $C_{\mathrm{L,wing}}$ = 0.5 - Clean sheet designs

The solid curves show the lift distributions resulting in a global lift coefficient of $C_{\mathrm{L,wing}}$ = 0.5. Compared to the corresponding curve in Fig. 12, the solid grey line shows smaller deviations from the target distribution. Therefore, the benefit from the LDM design is smaller and the zero twist design has acceptable results. For the lower lift coefficient of $C_{\mathrm{L,wing}}$ = 0.2, the LDM design originally optimized for $C_{\mathrm{L,wing}}$ = 0.5 starts deviating from the target ellipse. Although this is also expected for the LDM design from Sect. 5.1, the already smaller benefit disappears completely. This leads to the global drag polars presented in Fig. 19.

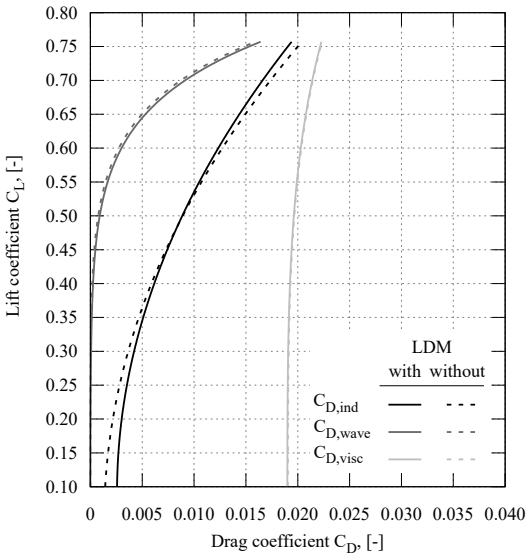

FIG 19. Global drag polars - Clean sheet designs

Again, the viscous drag does not change, and the wave drag shows similar behavior as in Sect. 5.1.1. The crossing point in the induced drag polar already present in Fig. 13 now occurs at $C_{\mathrm{L}} \approx 0.48$ and thus at lift coefficients relevant for cruise flight. It is important to highlight that all observed effects from Sect. 5.1.1 are also valid for the clean sheet designs. Hence, the course of the global induced drag polar is a combination of these effects and the already smaller benefit in the wing drag polar in Fig. 17. For an exemplary lift coefficient of C_{L} = 0.5, this even leads to a slightly worse L/D of 17.02 (with LDM) compared to 17.05 (without LDM). At this point, savings in $C_{\mathrm{D,ind}}$ are too small to compensate the increase of $C_{\mathrm{D,wave}}$.

Therefore, it is concluded that the pure approximation to an elliptical lift distribution for one design lift coefficient does not necessarily result in improved aerodynamics for the whole polar. Influential factors are not only the effects due to pitch trimming but also the initial twist distribution of the aircraft the LDM design is compared with. In the next section, the resulting overall performance is discussed.

5.2.2. Overall performance - Clean sheet design

The trajectory and C_{L} do not show any unexpected behavior, which is why an additional plot is omitted. In Fig. 20, the relative percentage change of relevant key parameters compared to the design without LDM is shown.

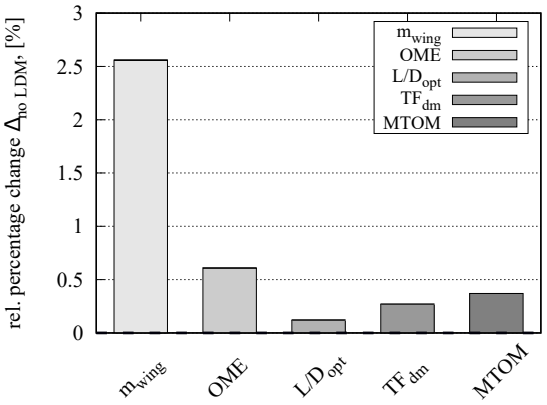

FIG 20. Relative percentage changes compared to clean sheet design without LDM

For the clean sheet design, the relative changes in wing mass and OME are less than for the reference design. This is due to the smaller deviations in the lift distributions and therefore smaller shift of the CoP due to the LDM (see Fig. 18). Again, the optimum C_{L} values slightly differ with $C_{\mathrm{L,opt}}$ = 0.533 for the design without LDM and $C_{\mathrm{L,opt}}$ = 0.541 for the LDM design; this results in the almost negligible increase in L/D_{opt} of 0.12 %. In contrast to the reference design, this aerodynamic benefit does not compensate the increased OME and consequently results in a 0.27 % increase in trip fuel mass and a 0.37 % increase in MTOM. Although these values are all comparatively small, this supports the previous statement and shows that simply approximating an elliptical lift distribution for a design lift coefficient does not necessarily result in improved overall aircraft performance.

6. CONCLUSION AND OUTLOOK

In this work, a straight forward approach to approximate given lift distributions for a known wing geometry was presented. The default procedure foresees the iterative adjustment of the twist based on residuals from LIFTING_LINE results. After describing the initial idea, the course of development of the method to its final status and first aerodynamic results for a short range reference wing were presented. Additionally, to judge the plausibility of the resulting twist distributions, LIFTING_LINE was replaced by the 3D panel method PANUKL. Although this method considers the local thicknesses of the wing, the results showed similar behavior. Since low computation time is a major advantage in conceptual aircraft design, the faster LIFTING_LINE approach was used for Sects. 4 and 5. Various tool-specific studies demonstrated both robustness and applicability for different input conditions, such as different wing geometries. The overall aircraft design studies revealed potential for a significant performance increase by approximating an elliptical lift distribution for the CSR-01 reference design; however, this statement is not universally valid. For the clean sheet design, several effects on both aerodynamics and structures actually led to poorer overall aircraft performance in terms of trip fuel consumption. Once again, the usual challenge in aircraft design is evident, as the designer should not optimize just one area, but find the optimal compromise between several disciplines. In future, the presented approach simplifies the setup of such optimization studies.

As a next step, the authors want to implement the 3D panel method PMARC to investigate the influence of the therein used function to consider the viscosity. Additionally, a relaxation of requirements could be investigated; for example, the criterion to achieve a perfect match between current and target lift distribution over the whole wing might lead to the unexpected behavior of the twist in the outer wing area. Finally, in the context of current research topics at ILR, the trade-off between aerodynamics and structures in conceptual aircraft design can be investigated. Of particular interest is the question whether prior adjustment of the twist distribution and the associated influence on the wing mass is more advantageous than designing the wing from a more structural point of view and increasing the aerodynamics in cruise flight using, e.g., variable camber technology.

Acknowledgements

The research presented in this publication has been conducted within the framework of the AVACON (Advanced Aircraft Concepts) project and has received funding from the Federal Aviation Research Programme LuFo V.3. We would like to acknowledge both the support of the Federal Ministery for Economic Affairs and Climate Action and the project partners for the valuable discussions. In addition, we thank all involved (former) colleagues and student assistants at ILR. Finally, we greatly appreciate the work of Yannik Cuypers in his excellent master's thesis.

Contact address

tim.effing@ilr.rwth-aachen.de

References

[1] Prandtl, L. "Über Tragflügel kleinsten induzierten Widerstandes". In: *Zeitschrift für Flugtechnik und Motorluftschiffahrt* 24, 1933, pp. 305–306.

[2] Torenbeek, E. *Synthesis of Subsonic Airplane Design*. Delft and Dordrecht, Netherlands: Delft University Press and Kluwer Academic Publishers, 1982.

[3] Raymer, D. P. *Aircraft design: A conceptual approach. AIAA Education Series*. Washington, DC: AIAA, 1992.

[4] Risse, K., Anton, E., Lammering, T., Franz, K., and Hoernschemeyer, R. "An Integrated Environment for Preliminary Aircraft Design and Optimization". In: *53rd AIAA/ASME/ASCE/AHS/ASC Structures, Structural Dynamics and Materials Conference: SciTech 2012*. Ed. by American Institute of Aeronautics and Astronautics. Vol. 2012-1675. AIAA, 2012.

[5] Schültke, F., Aigner, B., Effing, T., Strathoff, P., and Stumpf, E. "MICADO: Overview of Recent Developments within the Conceptual Aircraft Design and Optimization Environment". In: *69. Deutscher Luft- und Raumfahrtkongress*. Ed. by Deutsche Gesellschaft für Luft- und Raumfahrt - Lilienthal - Oberth e.V. 2020.

[6] Lock, C. N. H. *The Ideal Drag Due to a Shock Wave. Parts I and II*. Reports and Memoranda. Tech. rep. 2512. 1945.

[7] Boppe, C. W. "CFD Drag Prediction for Aerodynamic Design". In: *Technical Status Review on Drag Prediction and Analysis from Computational Fluid Dynamics: State of the Art*. Vol. AGARD-AR-256. Neuilly-sur-Seine, France: NATO AGARD, 1989.

[8] Drela, M. and Youngren, H. *Athena Vortex Lattice (AVL) 3.36 User Primer*. Tech. rep. [user guide]. Cambridge, MA: Massachusetts Institute of Technology, 2017.

[9] Horstmann, K.-H. *Ein Mehrfach-Traglinienverfahren und seine Verwendung für Entwurf und Nachrechnung nichtplanarer Flügelanordnungen*. Tech. rep. FB 87-51. Braunschweig, Germany: German Test and Research Institute for Aviation and Space Flight (DFVLR), 1987.

[10] Horstmann, K.-H., Engelbrecht, T., and Liersch, C. M. *LIFTING_LINE v3.0 Handbook*. Tech. rep. [user guide]. Braunschweig, Germany: DLR Institute of Aerodynamics and Flow Technology, 2019.

[11] Göthert, B. H. *Plane and Three-Dimensional Flow at High Subsonic Speeds*. Washington, DC, 1946.

[12] Schlichting, H. and Truckenbrodt, E. A. *Aerodynamik des Flugzeuges: Aerodynamik des Tragflügels (Teil II), des Rumpfes, der Flügel-Rumpf-Anordnung und der Leitwerke*. 3. Aufl. Vol. 2. Klassiker der Technik. Berlin: Springer, 2001.

[13] Liersch, C. M. and Wunderlich, T. "A Fast Aerodynamic Tool for Preliminary Aircraft Design". In: *12th AIAA/ISSMO Multidisciplinary Analysis and Optimization Conference*. Reston, Virigina: American Institute of Aeronautics and Astronautics, 2008.

[14] Derbyshire, T. and Sidwell, K. *PAN AIR Summary Document, (Version 1.0). NASA Contractor Report 3250*. Tech. rep. 1982.

[15] Warsaw University of Technology. *PANUKL: Version 2018: User manual*. Tech. rep. [user guide]. Warsaw, Poland: Faculty of Power Engineering and Aeronautics, 2017.

[16] McDonald, R. A. and Gloudemans, J. R. "Open Vehicle Sketch Pad: An Open Source Parametric Geometry and Analysis Tool for Conceptual Aircraft Design". In: *AIAA SCITECH 2022 Forum*. Reston, Virginia: American Institute of Aeronautics and Astronautics, 2022.

[17] Ashby, D. L., Dudley, M. R., Iguchi, S. K., Browne, L., and Katz, J. *Potential Flow Theory and Operation Guide for the Panel Code PMARC*. Ed. by National Aeronautics and Space Administration. 1991.

[18] Obert, E. *Aerodynamic Design of Transport Aircraft*. Amsterdam, Netherlands: IOS Press, 2009.

[19] Lane, K. A., Marshall, D. D., and McDonald, R. A. In: *48th AIAA Aerospace Sciences Meeting including the New Horizons Forum and Aerospace Exposition*. Ed. by American Institute of Aeronautics and Astronautics. 2010.

[20] Phillips, W. F., Hunsaker, D. F., and Joo, J. J. "Minimizing Induced Drag with Lift Distribution and Wingspan". In: *Journal of Aircraft* 56.2, 2019, pp. 431–441.

[21] Phillips, W. F. and Hunsaker, D. F. "Designing Wing Twist or Planform Distributions for Specified Lift Distributions". In: *Journal of Aircraft* 56.2, 2019, pp. 847–849.

[22] CeRAS. *Central Reference Aircraft data System*. Institute of Aerospace Systems (ILR), RWTH Aachen University, Aachen. URL: https://ceras.ilr.rwth-aachen.de.

[23] Risse, K., Schäfer, K., Schültke, F., and Stumpf, E. "Central Reference Aircraft data System (CeRAS) for research community". In: *CEAS Aeronautical Journal* 7.1, 2016, pp. 121–133.

[24] Woehler, S., Hartmann, J., Prenzel, E., and Kwik, H. "Preliminary aircraft design for a midrange reference aircraft taking advanced technologies into account as part of the AVACON project for an entry into service in 2028". In: *67. Deutscher Luft- und Raumfahrtkongress*. Ed. by Deutsche Gesellschaft für Luft- und Raumfahrt - Lilienthal - Oberth e.V. 2018.

[25] Elqatary, I. and Stumpf, E. "Structural Sizing For Preliminary Wing Mass Estimation of a Box-wing Aircraft". In: *6th Aircraft Structural Design Conference*. London: The Royal Aeronautical Society, 2018.

[26] Hafer, X. and Sachs, G. *Flugmechanik: Moderne Flugzeugentwurfs- und Steuerungskonzepte*. 3rd ed. Berlin: Springer, 1993.